

General theory of topological Hall effect in systems with chiral spin textures

K. S. Denisov,^{1,2,*} I. V. Rozhansky,^{1,2} N. S. Averkiev,^{1,2} and E. Lähderanta²

¹*Ioffe Institute, 194021 St.Petersburg, Russia*

²*Lappeenranta University of Technology, FI-53851 Lappeenranta, Finland*

(Dated: July 20, 2018)

We present a consistent theory of the topological Hall effect (THE) in 2D magnetic systems with disordered array of chiral spin textures, such as magnetic skyrmions. We focus on the scattering regime when the mean-free path of itinerant electrons exceeds the spin texture size, and THE arises from the asymmetric carrier scattering on individual chiral spin textures. We calculate the resistivity tensor on the basis of the Boltzmann kinetic equation taking into account the asymmetric scattering on skyrmions via the collision integral. Our theory describes both the adiabatic regime, when THE arises from a spin Hall effect and the non-adiabatic scattering when THE is due to purely charge transverse currents. We analyze the dependence of THE resistivity on a chiral spin texture structure, as well as on material parameters. We discuss the crossover between spin and charge regimes of THE driven by the increase of skyrmion size, the features of THE due to the variation of the Fermi energy, and the exchange interaction strength; we comment on the sign and magnitude of THE.

I. INTRODUCTION

Among rich variety of transport phenomena in magnetic materials the special attention is now focused on the topological Hall effect (THE). THE is the appearance of an additional transverse voltage due to itinerant carrier exchange interaction with chiral spin textures, such as magnetic skyrmions¹⁻⁴. THE has been extensively studied experimentally⁵⁻¹⁰ and has proved itself as an indicator of a non-zero chirality of the sample magnetization. The observation of THE has been reported for various systems exhibiting different chiral ordering of spins: skyrmion crystals⁹⁻¹², antiferromagnets (AFM)^{13,14}, spin glasses^{15,16} and disordered arrays of magnetic skyrmions^{5-7,17-21}.

Naturally, an appropriate microscopic theory of THE has to take into account the particular type of chiral spin ordering. In the case of a regular non-collinear spin structure with periodic or quasi-periodic spin arrangement, such as AFM lattices¹³ or skyrmion crystals^{9,22,23}, THE can be described in terms of an effective mean magnetic field^{9,24,25}. The meanfield approach is usually justified within the adiabatic approximation typical for systems with strong exchange coupling between the magnetization and the electrons carrying the current²⁶⁻³¹. Deviations from the condition of adiabaticity in THE due to long-ranged spin textures has been recently discussed in Ref.^{32,33}.

Another type of the chiral magnetization profiles studied experimentally is a disordered array of localized small spin textures spatially separated from each other^{7,18,34}. In this case a carrier moves freely most of the time, and the presence of localized magnetization vortices affects its trajectory by occasional scattering. The mean field approach is not adequate in this case as there is no regular long-range chiral spin structure which can be described by a homogeneous effective magnetic field. Instead, THE is driven by an asymmetric scattering of the carriers on individual spin textures being sensitive to their particular magnetization profile. The important feature of the in-

dividual scattering regime is that the properties of THE strongly depend on whether the carrier spin-flip processes are activated or not corresponding to so-called weak coupling regime and adiabatic regime, respectively³⁵. The transverse electric response arises from the spin Hall effect in the adiabatic regime and from the charge Hall effect in the weak coupling regime^{31,32,36-39}. Thus, the complete theory of THE for the irregular dilute chiral systems requires an accurate treatment of carrier scattering on a single chiral spin texture.

In this paper we develop the theory of the topological Hall effect in the diffusive regime for the dilute systems of localized magnetic textures. The approach is based on the consideration of asymmetric carrier scattering on individual spin textures. Our theory is applicable to disordered arrays of chiral spin textures with both electron spin subbands populated when THE can be generated both by charge and spin transverse currents. The paper is organized as follows: in section II the kinetic theory of THE is described accounting for the carrier scattering on host impurities and non-collinear spin textures, in section III the properties of the exchange asymmetric scattering are discussed, section IV covers the dependence of THE on material and spin texture parameters, we also describe the crossover between charge and spin Hall regimes of THE driven by the suppression of spin-flip scattering; in section V we summarize our results.

II. KINETIC THEORY

Let us consider two-dimensional degenerate electron gas (2DEG) described by the Hamiltonian:

$$\mathcal{H} = \frac{p^2}{2m} - \alpha_0 \mathbf{S}(\mathbf{r}) \cdot \boldsymbol{\sigma} + \sum_i u(\mathbf{r} - \mathbf{r}_i) \quad (1)$$

where the first term describes the electron free motion with an effective in-plane mass m , the second term represents the electrons exchange interaction with a magnetic

texture described by a static spin field $\mathbf{S}(\mathbf{r})$, where α_0 is an exchange coupling constant, $\boldsymbol{\sigma}$ is the vector of Pauli matrices, the last term describes scattering on host non-magnetic impurities located at \mathbf{r}_i . The topological Hall effect appears when $\mathbf{S}(\mathbf{r})$ has a non-collinear structure characterized by a non-zero spin chirality.

We consider the case, when the spin field $\mathbf{S}(\mathbf{r})$ consists of two contributions:

$$\mathbf{S}(\mathbf{r}) = S_0 \mathbf{e}_z + \sum_j \delta \mathbf{S}(\mathbf{r} - \mathbf{r}_j). \quad (2)$$

The first term is a background homogeneous field directed perpendicular to the 2DEG plane leading to the Zeeman spin splitting $\Delta = \alpha_0 S_0$. We assume ferromagnetic exchange ($\Delta > 0$) and that the Fermi energy exceeds the spin splitting so that both spin subbands are populated. The second contribution describes localized non-collinear spin textures $\delta \mathbf{S}$ of a few nanometer size located at \mathbf{r}_j and causing an additional elastic scattering of the carriers. While magnetic skyrmions are the typical example of a localized non-collinear spin texture, our consideration covers much wider class of chiral spin textures, not necessarily having a non-zero topological charge³⁵. The feature of the chiral spin structures is that for a given incident electron flux there is a difference in scattering rates to the left and to the right, eventually leading to the Hall effect.

We consider the classic transport regime ($k_F \ell \gg 1$ where $k_F = \sqrt{2mE_F}/\hbar$ is Fermi wave-vector, ℓ is the mean free path) on the basis of the Boltzmann kinetic equation:

$$e\mathbf{E} \cdot \frac{\partial f_s(\mathbf{p})}{\partial \mathbf{p}} = \text{St}[f_s(\mathbf{p})], \quad (3)$$

$$\text{St}[f_s(\mathbf{p})] = \sum_{\mathbf{p}', s'} \left(\mathcal{W}_{\mathbf{p}\mathbf{p}'}^{ss'} f_{s'}(\mathbf{p}') - \mathcal{W}_{\mathbf{p}'\mathbf{p}}^{s's} f_s(\mathbf{p}) \right),$$

where $f_s(\mathbf{p})$ is the distribution function, \mathbf{p} is 2D momentum and $s = \pm 1/2$ is the carrier spin projection on the axis normal to the motion plane, \mathbf{E} is an in-plane electric field, $\mathcal{W}_{\mathbf{p}\mathbf{p}'}^{ss'}$ is the elastic scattering rate from (\mathbf{p}', s') to (\mathbf{p}, s) state, and e is the electron charge. We solve Eq.(3) in linear approximation with respect to \mathbf{E} .

Expressing the scattering rate $\mathcal{W}_{\mathbf{p}\mathbf{p}'}^{ss'}$ in the form of the Fermi Golden Rule we assume that it has two contributions:

$$\mathcal{W}_{\mathbf{p}\mathbf{p}'}^{ss'} = \frac{2\pi}{\hbar} \left(n_i |u_{\mathbf{p}\mathbf{p}'}|^2 \delta_{ss'} + n_{sk} |T_{\mathbf{p}\mathbf{p}'}^{ss'}|^2 \right) \delta(\varepsilon_p^s - \varepsilon_{p'}^{s'}), \quad (4)$$

where the first term in brackets describes the electron spin-independent scattering on non-magnetic impurities, the second term is driven by the scattering on chiral spin textures; interference effects between the two types of scatterers are neglected. Here n_i, n_{sk} are the sheet densities of impurities and localized magnetic textures, respectively, $u_{\mathbf{p}\mathbf{p}'}$ is Fourier transform of the non-magnetic impurity potential $u(\mathbf{r})$ from Eq. (1), $T_{\mathbf{p}\mathbf{p}'}^{ss'}$ is the exact T -matrix of electron scattering on the spin texture, and the

delta-function ensures energy conservation in the elastic scattering, the energy spectrum is $\varepsilon_p^s = p^2/2m - s\Delta$. Two contributions can be distinguished in the square modulus of the T -matrix:

$$|T_{\mathbf{p}\mathbf{p}'}^{ss'}|^2 = \frac{1}{\nu^2} (\mathcal{G}_{ss'}(\theta) + \mathcal{J}_{ss'}(\theta)), \quad (5)$$

$$\mathcal{G}_{ss'}(\theta) = \mathcal{G}_{ss'}(-\theta) \quad \mathcal{J}_{ss'}(\theta) = -\mathcal{J}_{ss'}(-\theta).$$

$\mathcal{G}_{ss'}(\theta), \mathcal{J}_{ss'}(\theta)$ are dimensionless symmetric and asymmetric scattering rates, respectively, θ is the scattering angle, $\nu = m/2\pi\hbar^2$ is 2D density of states (per one spin). In the introduced notation we omit the dependence of $\mathcal{G}_{ss'}, \mathcal{J}_{ss'}$ on the scattering energy.

It is the asymmetric part $\mathcal{J}_{ss'}(\theta)$ of an electron scattering on chiral spin textures that gives rise to the transversal current as the scattering rates to the left and to the right become unequal. The scattering asymmetry acts as an effective magnetic field, which sign can be either the same for both spin projections of an incident electron, hence leading to a charge Hall effect, or opposite for the opposite electron spin projections, leading to the spin Hall effect. The properties of $\mathcal{J}_{ss'}(\theta)$ are discussed in Ref.³⁵ and summarized in Section III.

In order to solve the kinetic equation (3) we write $f_s(\mathbf{p}) = f_s^0 + g_s(\mathbf{p})$, where f_s^0 and g_s are the equilibrium and non-equilibrium parts of the distribution function, respectively. The external electric field \mathbf{E} is directed along x -axis. The angular dependence of $g_s(\mathbf{p})$ can be expressed as a sum of two terms, even and odd with respect to the angle:

$$g_s(\mathbf{p}) = g_s^+(p) \cos \varphi + g_s^-(p) \sin \varphi, \quad (6)$$

where φ is the momentum \mathbf{p} polar angle counted from x axis. After integrating the collision integral (3) over \mathbf{p}' we arrive at the following system of equations:

$$eE \begin{pmatrix} v_\uparrow \frac{\partial f_\uparrow^0}{\partial \varepsilon} \\ 0 \\ \frac{\partial f_\downarrow^0}{\partial \varepsilon} \\ v_\downarrow \frac{\partial f_\downarrow^0}{\partial \varepsilon} \\ 0 \end{pmatrix} = \begin{pmatrix} -\tau_\uparrow^{-1} & \Omega_{\uparrow\uparrow} & \tau_{\uparrow\downarrow}^{-1} & -\Omega_{\uparrow\downarrow} \\ -\Omega_{\uparrow\uparrow} & -\tau_\uparrow^{-1} & \Omega_{\uparrow\downarrow} & \tau_{\uparrow\downarrow}^{-1} \\ \tau_{\downarrow\uparrow}^{-1} & -\Omega_{\downarrow\uparrow} & -\tau_\downarrow^{-1} & \Omega_{\downarrow\downarrow} \\ \Omega_{\downarrow\uparrow} & \tau_{\downarrow\uparrow}^{-1} & -\Omega_{\downarrow\downarrow} & -\tau_\downarrow^{-1} \end{pmatrix} \begin{pmatrix} g_\uparrow^+ \\ g_\uparrow^- \\ g_\downarrow^+ \\ g_\downarrow^- \end{pmatrix}. \quad (7)$$

Here we introduced the following parameters:

$$\tau_s^{-1} = \tau_0^{-1} + \omega_s; \quad \tau_0^{-1} = n_i \frac{2\pi}{\hbar} \nu \int_0^{2\pi} |u_{\mathbf{p}\mathbf{p}'}|^2 (1 - \cos \theta) \frac{d\theta}{2\pi};$$

$$\omega_s = n_{sk} \frac{2\pi}{\hbar} \int_0^{2\pi} [(1 - \cos \theta) \mathcal{G}_{ss}(\theta) + \mathcal{G}_{\bar{s}s}] \frac{1}{\nu} \frac{d\theta}{2\pi};$$

$$\tau_{s\bar{s}}^{-1} = n_{sk} \frac{2\pi}{\hbar} \int_0^{2\pi} \mathcal{G}_{s\bar{s}}(\theta) \cos \theta \frac{1}{\nu} \frac{d\theta}{2\pi};$$

$$\Omega_{ss'} = \frac{eB_{ss'}}{mc}; \quad B_{ss'} = (n_{sk} \phi_0) \int_0^{2\pi} \mathcal{J}_{ss'}(\theta) \sin \theta d\theta, \quad (8)$$

where τ_s is the total transport lifetime, τ_0 is the transport lifetime for the scattering on non-magnetic impurities, ω_s^{-1} and $\tau_{s\bar{s}}$ are the transport lifetimes for the scattering on chiral textures (here \bar{s} is the spin subband index opposite to s). The transverse Hall current due to the asymmetrical scattering is related to the parameter $\Omega_{ss'}$, which is analogous to the cyclotron frequency in the ordinary Hall effect; $B_{ss'}$ is the corresponding effective magnetic field, $\phi_0 = hc/|e|$ is the magnetic flux quantum, c is the speed of light.

The coefficients g_s^μ ($\mu = \pm$) linearly depend on the electric field: $g_s^\mu = \mathcal{A}_s^\mu E$, where \mathcal{A}_s^μ can be obtained from Eq. (7) by inverting the collision integral matrix. The longitudinal σ_{xx}^s and transverse σ_{xy}^s conductivities within each spin subband s are given by:

$$\begin{aligned} \sigma_{xx}^s &= e\nu \int d\varepsilon \sqrt{\frac{\varepsilon}{2m}} \mathcal{A}_s^+(\varepsilon), \\ \sigma_{yx}^s &= e\nu \int d\varepsilon \sqrt{\frac{\varepsilon}{2m}} \mathcal{A}_s^-(\varepsilon), \\ \sigma_{xx} &= \sigma_{xx}^\uparrow + \sigma_{xx}^\downarrow, \quad \sigma_{yx} = \sigma_{yx}^\uparrow + \sigma_{yx}^\downarrow, \quad \hat{\rho} = \hat{\sigma}^{-1}; \end{aligned} \quad (9)$$

where the integration goes over the energy ε , $\hat{\rho}$ is the tensor of resistivity. The topological Hall effect is determined by \mathcal{A}_s^- . Let us stress out that both spin-conserving and spin-flip scattering channels contain asymmetric parts $\Omega_{ss'}$ and thus contribute to \mathcal{A}_s^- , and THE. Moreover, as there exist different regimes of THE³⁵, it might be necessary to calculate the exact scattering rates $\mathcal{J}_{ss'}$.

III. ASYMMETRIC ELECTRON SCATTERING ON A CHIRAL SPIN TEXTURE

In this section we consider the features of asymmetric electron scattering on a single non-collinear magnetic texture. We express the scattering potential in the form:

$$V(\mathbf{r}) = -\alpha_0 \delta \mathbf{S}(\mathbf{r}) \cdot \boldsymbol{\sigma}. \quad (10)$$

Outside the localized spin texture of a characteristic diameter a the magnetization is unperturbed so that $\delta \mathbf{S}(r > a/2) \rightarrow 0$ and the scattering potential vanishes. The topological Hall effect appears due to the asymmetry in the electron scattering when the potential (10) can be characterized by a non-zero chirality. The details of the asymmetric scattering depend on the particular distribution of spins in the texture and its size as well as on the exchange interaction strength and the incident electron wavevector³⁵.

A. Chiral spin textures

To describe a non-collinear spin texture in 2D the following parametrization is commonly used:

$$\delta \mathbf{S}(\mathbf{r}) = \begin{pmatrix} \delta S_{\parallel}(r) \cos(\varkappa\phi + \gamma) \\ \delta S_{\parallel}(r) \sin(\varkappa\phi + \gamma) \\ \delta S_z(r) \end{pmatrix} \quad (11)$$

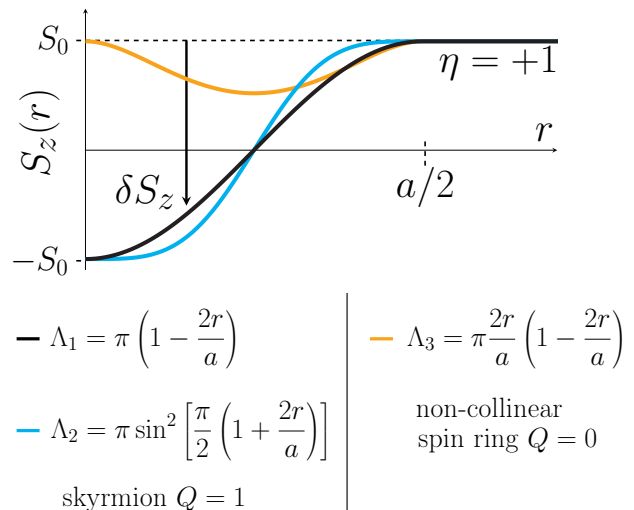


FIG. 1: The typical profiles $S_z(r) = S_0 \cos \Lambda(r)$ of non-collinear spin textures. Note that for $\eta = +1$, the $\delta S_z(r) < 0$ is negative.

where $\mathbf{r} = (r, \phi)$ is the polar radius-vector, $r = 0$ corresponds to the center of the texture. The functions $\delta S_{\parallel}, \delta S_z \neq 0$ depend on the distance from the center r . The vorticity \varkappa describes the in-plane spin rotation with an initial phase γ . In what follows we consider that δS_z is counted from the background magnetization S_0 , whose sign we denote as $\eta = \text{sgn}(S_0)$. In the last section we will also consider the case when S_0 and δS_z are independent.

Fig. 1 shows the profiles $S_z(r) = S_0 \cos \Lambda(r)$ for three examples of chiral spin textures with $\eta = +1$ (we assume that $\delta S_{\parallel}^2 = S_0^2 - S_z^2$). Two of them describe a magnetic skyrmion ($\Lambda_1(r) = \pi(1 - 2r/a)$, $\Lambda_2(r) = \pi \sin^2[(\pi/2)(1 + 2r/a)]$). The skyrmion has opposite sign of spins in its center with respect to the background magnetization, which leads to the appearance of a nonzero topological charge called winding number Q . The nonzero Q is particularly important for the thermal stability of skyrmions in ferromagnetic thin films^{40–47}. The third magnetization profile Fig. 1 ($\Lambda_3(r) = (2r/a)\pi(1 - 2r/a)$) corresponds to a non-collinear spin ring with the orientation of spins in the center parallel to S_0 . Non-collinear rings have zero winding number, but they exhibit a similar topological Hall effect³⁵. Such spin textures can appear in a material with spin-orbit interaction functionalized by magnetic impurities, in a vicinity of a defect or impurity^{34,48–50}. Let us notice that for the positive background spin orientation ($\eta = +1$) δS_z is negative.

Substituting (11) into (10) we get for the scattering potential:

$$V(\mathbf{r}) = -\alpha_0 \begin{pmatrix} \delta S_z(r) & e^{-i\varkappa\phi - i\gamma} \delta S_{\parallel}(r) \\ e^{i\varkappa\phi + i\gamma} \delta S_{\parallel}(r) & -\delta S_z(r) \end{pmatrix}. \quad (12)$$

The potential $V(\mathbf{r})$ is a 2×2 matrix, which depends on a polar angle ϕ via the off-diagonal components. When

both functions S_z, S_{\parallel} are non-zero, the angular dependence of the potential leads to the appearance of the asymmetric part in electron scattering rates $\mathcal{J}_{ss'}(\theta) = -\mathcal{J}_{ss'}(-\theta)$, where θ is the scattering angle. The sign of $\mathcal{J}_{ss'}$ depends on \varkappa , while the constant phase γ plays no role in the scattering. The role of η is more complicated; we further explicitly specify the dependence of $\mathcal{J}_{ss'}$ on η .

B. Asymmetric scattering features

We consider the case when Fermi energy exceeds the background exchange splitting $E_F > \Delta/2$ so that both spin subbands are populated with electrons ($\Delta = \alpha_0 S_0$). The symmetry upon the time inversion allows us to present the asymmetric scattering rates $\mathcal{J}_{ss'}(\theta, \eta)$ introduced in Eq. (5) in the form (see the details in Appendix A):

$$\begin{aligned}\mathcal{J}_{\uparrow\uparrow}(\theta, \eta) &= \eta\Gamma_1(\theta) + \Pi(\theta), \\ \mathcal{J}_{\downarrow\downarrow}(\theta, \eta) &= \eta\Gamma_1(\theta) - \Pi(\theta), \\ \mathcal{J}_{\uparrow\downarrow}(\theta, \eta) &= \mathcal{J}_{\downarrow\uparrow}(\theta, \eta) = \eta\Gamma_2(\theta),\end{aligned}\quad (13)$$

where $\Gamma_{1,2}(\theta)$ and $\Pi(\theta)$ have no dependence on η . This representation is convenient for treating the topological charge and spin Hall effects independently. Indeed, the terms $\eta\Gamma_{1,2}$ describe the asymmetric scattering in the same transverse direction determined by the texture orientation η and independent of an initial carrier spin state. These terms, therefore, lead to the charge Hall effect. On the contrary, the term Π describes the scattering of spin up and spin down electron in the opposite transverse directions independent of η . This process leads to spin Hall effect, it is absent for spin-flip channels. Both $\Gamma_{1,2}$ and Π change their sign upon $\varkappa \rightarrow -\varkappa$.

Which of the two contributions to the topological Hall effect (charge or spin) dominate strongly depends on whether the spin-flip processes are activated or not. Away from the threshold $E_F \gg \Delta/2$ the rate of the spin-flip scattering is controlled by the adiabatic parameter $\lambda_a = (\alpha_0 S_0/\hbar)\tau_a$, where $\tau_a = a/v_F$ is an electron time of flight through the texture of diameter a with Fermi velocity $v_F = \sqrt{2E_F/m}$.

In the case of $\lambda_a \leq 1$ the spin-flip processes are effective, the asymmetric scattering arises from the interference between double spin-flip and single spin-conserving scattering events (so-called spin-chirality driven mechanism^{32,36-39}). This process is sensitive to the spin chirality χ defined for any three spins $\delta\mathbf{S}_1, \delta\mathbf{S}_2, \delta\mathbf{S}_3$ forming the spin texture as $\chi = \text{sgn}(\delta\mathbf{S}_1 \cdot [\delta\mathbf{S}_2 \times \delta\mathbf{S}_3])$. The non-zero chirality of the spin texture in the weak coupling regime leads to the charge Hall effect. The spin chirality based contribution is described by $\Gamma_{1,2}$. At $\lambda_a \leq 1$ these terms dominate $\Gamma_{1,2} \gg \Pi$, with spin-flip scattering prevailing $\Gamma_2 = 2\Gamma_1$.

In the opposite case of large adiabatic parameter $\lambda_a \gg 1$ the spin flip processes are suppressed in accordance with the adiabatic theorem. In this regime the scattering asymmetry is due to the Berry phase acquired

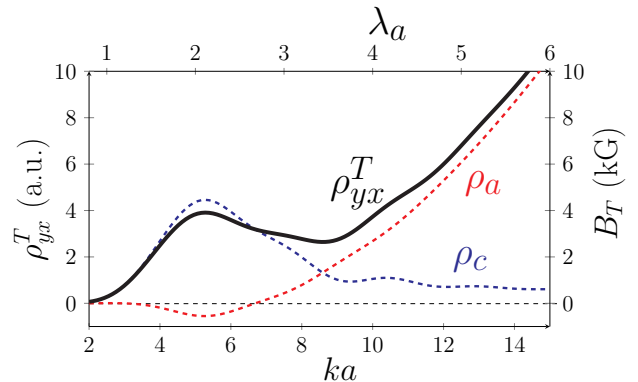


FIG. 2: The dependence of ρ_{yx}^T on magnetic skyrmion diameter ka for Λ_1 profile, and the crossover between charge and spin topological Hall effect. The parameters $P_s = 0.4$, $n_{sk} = 2 \times 10^{11} \text{ cm}^{-2}$.

by the wave-function of electron moving through a non-collinear spin field. The hallmark of this mechanism is that the sign of the effective magnetic field associated with the Berry phase appears to be opposite for spin up and spin down electrons, thus leading to the spin Hall effect^{24,28,30,31}. This adiabatic contribution to the Hall response is, therefore, described by Π . At $\lambda_a \gg 1$ the spin Hall effect dominates $\Pi \gg \Gamma_{1,2}$, and the charge Hall effect appears only due to nonzero carrier spin polarization P_s .

The interplay between charge and spin topological Hall effects leads to a few nontrivial features discussed in the following section.

IV. TOPOLOGICAL HALL EFFECT

In this section we discuss the topological contribution to the Hall resistivity ρ_{yx}^T in the diffusive regime for different systems.

A. Dilute array of chiral spin textures

Let us consider a two-dimensional film containing spatially localized chiral spin textures such as magnetic skyrmions or non-collinear magnetic rings (see Fig. 1). We assume that all the textures have the same vorticity \varkappa , and the orientation $\eta = \text{sgn}(S_0) = +1$ is fixed, being determined by the background magnetization S_0 . We consider the dilute regime, when the scattering rate on spin textures is much smaller than that on non-magnetic impurities $\omega_s \tau_0 \ll 1$, $\Omega_{ss'} \tau_0 \ll 1$, so the transport lifetime is given by $\tau_s = \tau_0$. Solving the system (7) for \mathcal{A}_s^- in the lowest order in $(\Omega_{ss'} \tau_0)$ we express the topological

Hall resistivity ρ_{yx}^T as a sum of two contributions:

$$\begin{aligned}\rho_{yx}^T &= \rho_c + \rho_a, \\ \rho_c &= \frac{1}{nec} (\phi_0 n_{sk}) \int_0^{2\pi} (\Gamma_1 + \Gamma_2) \sin \theta d\theta; \\ \rho_a &= P_s \frac{1}{nec} (\phi_0 n_{sk}) \int_0^{2\pi} \Pi \sin \theta d\theta.\end{aligned}\quad (14)$$

The term ρ_c describes the charge transverse current (charge Hall effect) generated due to carrier asymmetric scattering due to spin-independent terms $\Gamma_{1,2}$ (see Eq. 13). The term ρ_a describes the transverse spin current (spin Hall effect) driven by the spin-dependent contribution to the asymmetric scattering Π (Eq. 13). The spin current does not lead to a charge separation unless there is unequal number of spin up and spin down carriers in the system. Therefore, this contribution to the Hall resistivity is proportional to the carrier spin polarization $P_s = (n_\uparrow - n_\downarrow)/(n_\uparrow + n_\downarrow) = \Delta/2E_F$. In Eq. 14 the notation n stands for 2DEG sheet density.

The relative importance of the two contributions ρ_a and ρ_c in the appearance of the transverse charge current depends on the texture diameter a or the Fermi level E_F as discussed in the following sections.

1. Crossover between charge and spin Hall effect

Let us trace the dependence of ρ_{yx}^T (14) on the spin texture diameter a . We assume that the Fermi energy E_F substantially exceeds the exchange spin splitting so that both spin subbands are populated and the spin polarization of the carriers is far below 100%: $P_s = \Delta/2E_F \ll 1$. In this case the rate of spin-flip processes are fully controlled by λ_a . The adiabatic parameter can be expressed as $\lambda_a = P_s(ka)$, where $k = \sqrt{2E_F m/\hbar^2}$. When spin-flip scattering is activated the topological Hall effect is dominated by the transverse charge currents ($\rho_c \gg \rho_a$ at $\lambda_a \leq 1$), due to the spin-chirality driven mechanism. In the opposite case $\rho_a \gg \rho_c$ the transverse current appears due to spin Hall effect induced by the adiabatic Berry phase mechanism. This regime is set when the spin-flip channels are suppressed at $\lambda_a \gg 1$. With the change of the texture diameter a from small to large values a crossover occurs between the charge Hall and spin Hall dominated regimes. In addition, the change of the texture size affects the wave parameter ka , which determines the properties of the scattering related to the electron relation between the electron wavelength and the scatterer size. With these two consequences of the texture size variation acting simultaneously, the topological Hall resistivity ρ_{yx}^T necessarily exhibits a non-monotonic dependence on ka .

Fig. 2(b) shows the calculated dependence of charge ρ_c , adiabatic ρ_a and total ρ_{yx}^T topological Hall resistivity

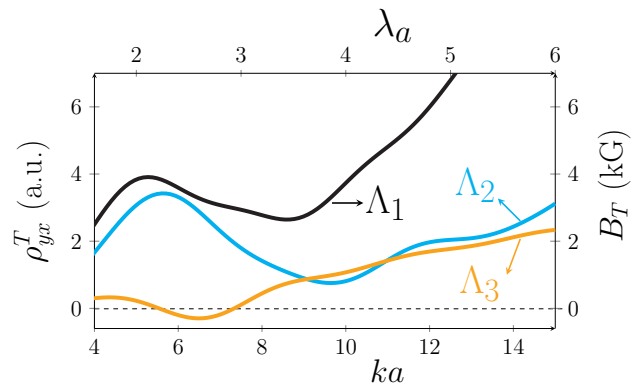


FIG. 3: The dependence of ρ_{yx}^T on chiral texture diameter ka for different texture profiles in the region of crossover. The parameters $P_s = 0.4$, $n_{sk} = 2 \times 10^{11} \text{ cm}^{-2}$.

on the skyrmion diameter a for the magnetic skyrmion with magnetization spatial profile $\Lambda_1(r)$ shown in Fig. 1. For the calculation results shown in Fig. 2 the spin polarization was taken $P_s = 0.4$, and the skyrmion sheet density $n_{sk} = 2 \times 10^{11} \text{ cm}^{-2}$. The scattering rates $\mathcal{J}_{ss'}$ were calculated using the phase function method³⁵.

As can be seen in Fig. 2, for $\lambda_a \leq 1.8$ the charge contribution ρ_c exceeds ρ_a , at that ρ_{yx}^T is dominated by the purely charge current. For $\lambda_a \geq 4.5$ the adiabatic term prevails $\rho_a \gg \rho_c$ and ρ_{yx}^T appears due to the spin current converted into the charge current. As was discussed above, indeed ρ_{yx}^T appears to be non-monotonic when the crossover between ρ_c and ρ_a occurs in the range ($1.8 \gtrsim \lambda_a \gtrsim 4.5$). As the spin-flip processes are suppressed, firstly the charge contribution ρ_c is decreased, and only later the adiabatic term ρ_a starts to increase. This effect results in the appearance of local minimum for ρ_{yx}^T in the crossover regime.

The behaviour of ρ_{yx}^T in the crossover regime is highly sensitive to a particular magnetic texture profile. In Fig. 3 we present the dependence of ρ_{yx}^T on a for three different spin texture spatial profiles shown in Fig. 1. As can be seen in Fig. 3 the oscillating structure of ρ_{yx}^T upon increasing ka exhibits a significant variation even for two very similar skyrmion configurations Λ_1 and Λ_2 . The strong dependence of ρ_{yx}^T on $\Lambda(r)$ observed in the crossover regime is due to the significance of the interference in electron scattering as the wave parameter $ka \sim \pi$ (Ref.³⁵). The texture described by Λ_2 has larger spin gradients, so the adiabatic term activates at larger ka , and the magnitude of ρ_{yx}^T for Λ_2 in the crossover regime is smaller than that of Λ_1 .

We would also like to stress out that the topological Hall effect exists as well due to scattering on non-collinear spin rings having zero winding number (orange curve in Fig. 3). The transverse conductivity ρ_{yx}^T due to scattering on non-collinear spin rings possesses all the features described above including the the existence of charge and

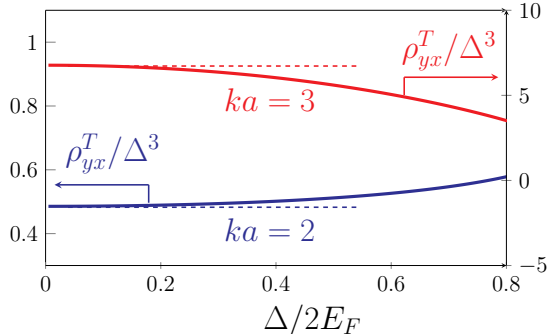


FIG. 4: The dependence of ρ_{yx}^T/Δ^3 on the variation of $\Delta/2E_F$ at $ka = 2$ (blue curve) and $ka = 3$ (red curve) for Λ_1 profile.

spin Hall limiting regimes.

2. The magnitude of the topological Hall effect

The magnitude of THE for the dilute systems can be expressed in terms of the effective magnetic field B_T introduced as:

$$\rho_{yx}^T = \frac{B_T}{nec}. \quad (15)$$

The field B_T shows the magnitude of the external magnetic field applied to the sample, at which the ordinary Hall effect contribution to the transverse resistivity ρ_{yx}^O becomes comparable with ρ_{yx}^T .

Usually in the THE estimates it is assumed that each skyrmion contributes via a magnetic flux quantum²¹. However, our analysis shows that such an estimate does not take into account the important features of the scattering. According to Eqs. (14),(15), ρ_{yx}^T and B_T linearly depend on both the skyrmion sheet density n_{sk} and the dimensionless scattering rates $\mathcal{J}_{ss'}$. Therefore, the actual magnitude of B_T is renormalized differently depending on the scattering regime. The scattering rates $\mathcal{J}_{ss'}$ are small at $\lambda_a \leq 1$, of the order of unity at an intermediate $\lambda_a \sim 1$, and reach the order of tens at $\lambda_a \gg 1$.

The magnitude of B_T for $n_{sk} = 2 \times 10^{11} \text{ cm}^{-2}$ can be seen in Figs. 2-6. At $n_{sk}\phi_0 \approx 8 \text{ T}$ the value of B_T in the intermediate regime is of the order of several kG; in the strong coupling regime ($\lambda_a \gg 1$) it can go as high as several Tesla⁵¹.

In the weak coupling regime ρ_{yx}^T scales as Δ^3 , as the perturbation theory couples ρ_{yx}^T with spin chirality and, therefore, THE requires the third order in the exchange interaction. In Fig. 4 the quantity ρ_{yx}^T/Δ^3 is shown for two values of $ka = 2, 3$. As can be seen from the figure, the scaling Δ^3 holds up to $\Delta/2E_F \approx 0.2$, the deviation from the scaling relation indicates that the perturbation theory becomes invalid departing from the weak coupling regime.

Let us note, that although the asymmetrical scattering rates $\mathcal{J}_{ss'}$ are small in the weak coupling regime due to the strong dependence on the exchange interaction strength Δ ($\mathcal{J}_{ss'}$ is proportional to $(\Delta/2E_F)^3(ka)^8$ at $\lambda_a \ll 1$), the magnitude of B_T can be large due to higher spin textures sheet density. For example, for $n_{sk} = 5 \times 10^{12} \text{ cm}^{-2}$ and $\lambda_a = 0.8$ ($ka = 2$, $P_s = 0.4$) one gets $B_T \approx 0.7 \text{ T}$.

3. The sign of the topological Hall effect

In a real experiment when electron transport in a system with non-collinear spin textures is studied as a function of the external magnetic field B_0 , it is often difficult to extract different contributions to the Hall effect. The total transverse resistivity ρ_{yx} contains three contributions $\rho_{yx} = \rho_{yx}^O + \rho_{yx}^A + \rho_{yx}^T$, where $\rho_{yx}^O, \rho_{yx}^A, \rho_{yx}^T$ are attributed to the ordinary, anomalous and topological Hall effects respectively. Here we focus on the sign difference between $\rho_{yx}^T = (B_T/nec)$ and $\rho_{yx}^O = (B_0/nec)$, thus we should compare the signs of B_T and B_0 .

We assume, that the background magnetization S_0 is directed along the external magnetic field $B_0 > 0$. In general, there is now any fixed relation between the signs of the topological Hall resistivity ρ_{yx}^T , charge ρ_c and adiabatic ρ_a contributions as can be seen in Fig. 2 and Fig. 3. In these figures ρ_a and ρ_{yx}^T for Λ_3 spin configuration change their signs upon increase of ka in the crossover region. However, it is possible to specify the sign of B_T in the limiting regimes, i.e. away from the threshold $E_F \gg \Delta/2$ and outside the adiabatic crossover $\lambda_a \approx 1$. Let us consider the weak coupling regime ($\lambda_a \leq 1$), in which the charge current contribution to THE dominates ($\rho_c \gg \rho_a$). In this regime, the effective magnetic field is proportional to the chirality of the spin texture $B_T \propto \delta\mathbf{S}_1 \cdot [\delta\mathbf{S}_2 \times \delta\mathbf{S}_3]$. For $\varkappa = +1$, $\eta = +1$ the sign of the mixed vector product of any three spins $\delta\mathbf{S}_1, \delta\mathbf{S}_2, \delta\mathbf{S}_3$ forming the skyrmion is negative and $B_T < 0$ due to $\delta S_z < 0$ (see Fig. 1), thus the sign of B_T appears to be opposite to B_0 . In the adiabatic regime ($\rho_a \gg \rho_c$) the electrons with positive spin projection (co-aligned with S_0) retain the same type of scattering asymmetry as for small λ_a . As these electrons constitute the majority at a positive spin polarization ($P_s > 0$), the effective magnetic field is also negative $B_T < 0$.

We conclude, that for $\varkappa = +1$, $\eta = +1$ configurations, the topological field B_T usually has the opposite sign to the sign of the external field B_0 . For chiral spin configurations with negative vorticity $\varkappa < 0$ the fields B_T and B_0 have the same sign. However, in the crossover regime $\lambda_a \sim 1$ and near the threshold $E_F \approx \Delta/2$ there is no any fixed relation between B_0 and B_T signs.

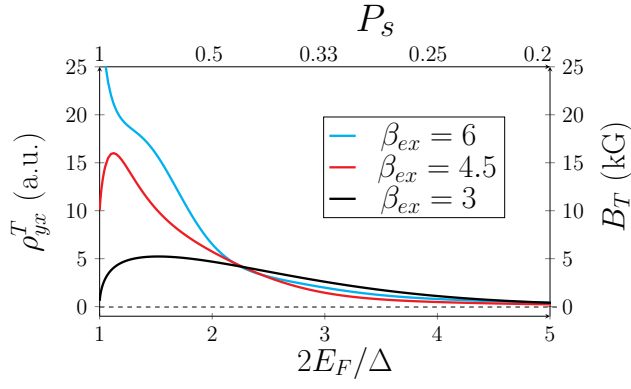


FIG. 5: The dependence of ρ_{yx}^T on Fermi energy E_F at different $\beta_{ex} = \sqrt{m\Delta/\hbar^2}a$ parameter for Λ_1 profile.

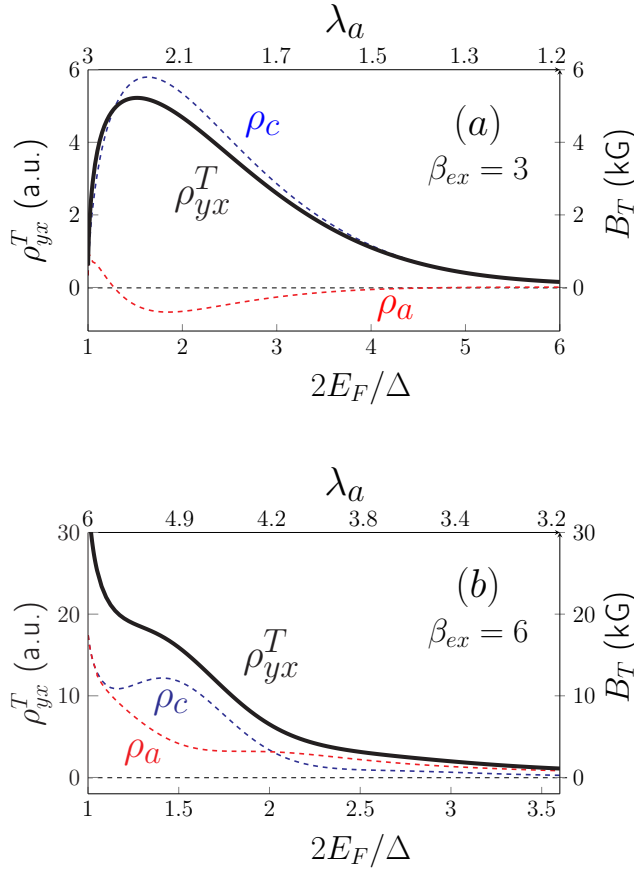


FIG. 6: The dependence of ρ_{yx}^T , ρ_c , ρ_a on Fermi energy E_F at $\beta_{ex} = 3$ (a) and $\beta_{ex} = 6$ (b) for Λ_1 profile.

4. Effect of the Fermi energy variation

The dependence of ρ_{yx}^T on the variation of the Fermi energy E_F exhibits a number of distinctive features. At $E_F < \Delta/2$ only one spin subband is occupied and spin polarization is $P_s = 1$. We start the analysis from the

threshold $E_F \geq \Delta/2$, when the electrons start populating the second spin subband. In further consideration we keep Δ and a constant changing only the Fermi energy E_F , which we express through the dimensionless parameter $2E_F/\Delta = P_s^{-1}$. We also introduce a dimensionless spin texture diameter $\beta_{ex} = \sqrt{m\Delta/\hbar^2}a$, it is independent of E_F . Fig. 5 shows the dependence of ρ_{yx}^T on $2E_F/\Delta$ and P_s calculated for the Λ_1 skyrmion configuration for three different values of β_{ex} . As can be seen from the figure, ρ_{yx}^T depends non-monotonically on $2E_F/\Delta$, with a maximum near the threshold and decreasing at a larger E_F . The suppression of ρ_{yx}^T at a large E_F is due to destructive scattering interference at $P_s \ll 1$ and $ka \gg 1$ (see Ref.³⁵). The magnitude of ρ_{yx}^T near the threshold is controlled by β_{ex} . As the spin-chirality driven mechanism relevant for a small skyrmion size does not work at $E_F < \Delta/2$ (there is no spin flip processes below the spin down subband edge), the decrease of β_{ex} suppresses ρ_{yx}^T at $E_F = \Delta/2$. These features of ρ_{yx}^T are specific to THE and can be possibly used to distinguish it from AHE and OHE contributions.

The variation of the Fermi energy affects the asymmetric part of the scattering cross-section simultaneously through ka and P_s factors and, therefore, gives rise to a number of interesting features in the transverse resistivity behaviour. We demonstrate these peculiarities in Fig. 6, where the dependence of ρ_{yx}^T , ρ_c , and ρ_a on $2E_F/\Delta$ is plotted for $\beta_{ex} = 3$ and $\beta_{ex} = 6$. The variation of E_F directly affects the adiabatic parameter, which can be expressed as $\lambda_a = \beta_{ex}\sqrt{P_s}$. For $\beta_{ex} = 3$ (Fig. 6a) the adiabatic term ρ_a is negative when far from the threshold. This is due to the complex scattering pattern typical for the intermediate range of the adiabatic parameter values ($1 \leq \lambda_a \leq 2$). We have already encountered this effect considering the behaviour of THE in the crossover regime: ρ_a is negative in Fig. 2 for the same range of λ_a as in Fig. 6a. For $\beta_{ex} = 6$ (Fig. 6b) λ_a is larger and the interference in the carrier scattering manifests itself through the oscillation of ρ_c , ρ_a magnitudes superimposed on the global suppression upon increasing of E_F . The same oscillating peculiarities of transverse response can be seen in Fig. 2 in the range $4 \leq \lambda_a \leq 5$.

Let us finally comment on the scattering rates behaviour in the vicinity of the threshold $E_F \approx \Delta/2$. Since the spin down and spin flip scattering channels are absent below the threshold $E_F < \Delta/2$, we conclude that at $E_F \approx \Delta/2$ the following relations are fulfilled: $\Gamma_2 \approx 0$, and $\Gamma_1(\theta) \approx \Pi(\theta)$. At that, only spin up scattering channel is activated with $\mathcal{J}_{\uparrow\uparrow} \approx 2\Pi(\theta)$ (i.e. $\rho_a \approx \rho_c$).

B. Dense array of skyrmions

In this section we apply the diffusive theory of THE to the case when the dominating scattering mechanism changes from scattering on non-magnetic impurities to scattering on magnetic textures. This transition takes place, for example, in ferromagnetic films in the vicinity

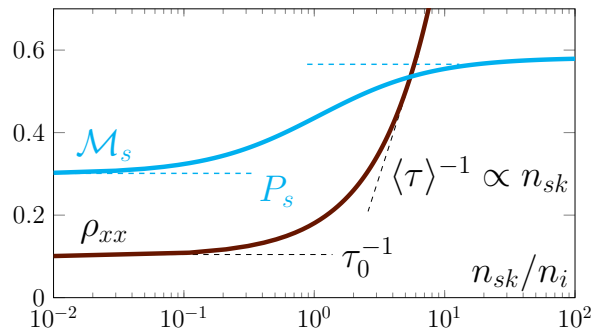


FIG. 7: The dependence of ρ_{xx} and \mathcal{M}_s on skyrmion sheet density n_{sk} .

of phase transition⁵², when the sheet density of thermally activated chiral magnetic fluctuations increases^{19,26,53}. The exchange interaction between free carriers and localized magnetic moments is typically strong in these systems so that the adiabatic approximation for THE is applicable. At that, the spin-flip scattering channels are completely suppressed ($\Omega_{\uparrow\downarrow} = \tau_{\uparrow\downarrow}^{-1} = 0$), and THE originates solely from the spin Hall effect ($\rho_a \gg \rho_c$).

The switching of the dominant scattering mechanism affects the spin dependent scattering time τ_s (Eq. 8). In the dilute regime of low skyrmion density $\omega_s \tau_0 \ll 1$ considered in the previous section, the total transport scattering time τ_s is independent of the carrier spin, being determined by scattering on host non-magnetic impurities $\tau_s = \tau_0$. Increasing the skyrmion sheet density turns the system into the dense skyrmionic regime $\omega_s \tau_0 \gg 1$, when the total transport scattering time is determined solely by the magnetic skyrmions and, hence, depends on the carrier spin state $\tau_s = \omega_s^{-1}$. This transition affects both the longitudinal and transverse resistivities. Even in the dense skyrmionic regime the magnitude of $\Omega_{ss} \tau_s \approx \Omega_{ss} / \omega_s$ remains small, as the symmetric scattering is more effective than the asymmetric one⁵¹. Thus, we can still solve the kinetic equation in the lowest order in $\Omega_{ss} \tau_s$ as described in the previous section.

Since the spin-flip processes are suppressed in the adiabatic regime, the spin up and spin down channels are uncoupled and contribute independently to the conductivity. Keeping only the leading terms with respect to $\Omega_{ss} \tau_s$ we get for the resistivity tensor:

$$\rho_{xx} = \frac{m}{ne^2 \langle \tau \rangle}, \quad \rho_{yx}^T = \mathcal{M}_s \frac{1}{nec} (\phi_0 n_{sk}) \int_0^{2\pi} \Pi \sin \theta d\theta,$$

$$\langle \tau \rangle = \frac{1}{2} [(1 + P_s) \tau_{\uparrow} + (1 - P_s) \tau_{\downarrow}],$$

$$\mathcal{M}_s = \frac{1}{2} \left[(1 + P_s) \frac{\tau_{\uparrow}^2}{\langle \tau \rangle^2} - (1 - P_s) \frac{\tau_{\downarrow}^2}{\langle \tau \rangle^2} \right]. \quad (16)$$

Here $P_s = (n_{\uparrow} - n_{\downarrow}) / (n_{\uparrow} + n_{\downarrow})$ is the spin polarization

of the 2D free carriers. We have also introduced an averaged scattering time $\langle \tau \rangle$. The introduced parameter \mathcal{M}_s controls the conversion of the spin Hall to the charge Hall current.

In Fig. 7 we plot the dependence of ρ_{xx} and the spin/charge Hall factor \mathcal{M}_s on the skyrmion sheet density n_{sk} via the parameter $\omega_s \tau$ covering the transition between scattering on non-magnetic impurities and skyrmions. In the dilute regime $\langle \tau \rangle = \tau_0$, and ρ_{xx} does not depend on n_{sk} . When τ_{ss}^{-1} exceeds τ_0 , the longitudinal resistivity $\rho_{xx} \propto \langle \tau \rangle^{-1}$ increases linearly with n_{sk} as shown in Fig. 7. From the experimental point of view this transition leads to the peak in resistivity upon increase of the temperature in the vicinity of the phase transition.

According to Eq. (16) the topological Hall resistivity ρ_{yx}^T is proportional to the skyrmion sheet density n_{sk} . The crossover in the dominating scattering mechanism affects ρ_{yx}^T only via the \mathcal{M}_s -factor. In the dilute regime ($\omega_s \tau_0 \ll 1$) this parameter coincides with the carrier spin polarization $\mathcal{M}_s = P_s$ as the scattering time on host impurities τ_0 is spin independent. However, in the dense regime ($\omega_s \tau_0 \gg 1$) the scattering time τ_s depends on the carrier spin, this dependence creates an additional spin imbalance favoring the conversion of spin to charge currents. As a result, the \mathcal{M}_s -factor is renormalized accounting for $\tau_{\uparrow} \neq \tau_{\downarrow}$.

Let us mention, that to describe dependence of the resistivities ρ_{xx}, ρ_{yx} on temperature and external magnetic field in the vicinity of FM-transition one should specify a specific model of skyrmion/antiskyrmion creation adequate for the considered material system.

The general expressions for ρ_{xx} and ρ_{yx}^T in the adiabatic regime (16) are applicable for any spin-dependent scattering mechanisms, not necessarily due to skyrmions. We point out, that in the leading order with respect to $\Omega_{ss} \tau_s$ the effect of τ_s on ρ_{yx}^T can be fully described by the replacement of the carriers spin polarization P_s by an effective \mathcal{M}_s -factor, which accounts for $\tau_{\uparrow} \neq \tau_{\downarrow}$.

C. Paramagnetic chiral systems

In the previous sections we considered THE in a 2D magnetic layer with a background magnetization S_0 and local deviations forming chiral magnetic textures. Unlike anomalous Hall effect, THE does not necessarily require macroscopic spin polarization of the carriers in the sample. Therefore, THE is allowed in a system with no background magnetization provided it still has localized chiral spin textures. We will refer to this situation as to a chiral paramagnetic case. In the absence of a preferred magnetization direction the chiral spin textures with opposite orientations can be created in the same sample. A few special features of ρ_{yx}^T are expected in such a case.

One scenario leading to a chiral paramagnetic system with two independent spin orientations has been recently proposed on the basis of a magnetic polaron (BMP) in a semiconductor³⁴. BMP is a collective state of a carrier

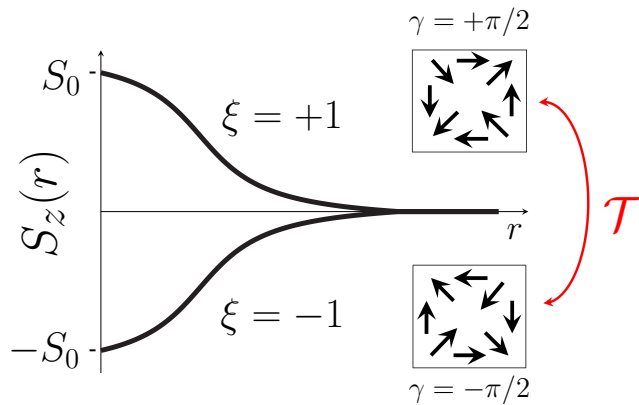


FIG. 8: Two chiral spin textures with opposite orientation $\xi = \pm 1$ and $\gamma = -1$ connected by the time-inversion \mathcal{T} .

localized at an impurity center and other paramagnetic impurities lying within the localization radius. Due to the exchange interaction the carrier polarizes other magnetic impurities within its wavefunction radius; at that a non-collinear spin structure of a chiral BMP appears due to the spin-orbit splitting of the carrier band states. This effect can be viewed as a case of Dzyaloshinskii-Moriya interaction mediated by a localized electron state. There are two opposite orientations of the spin field forming chiral BMP connected by time inversion symmetry. We denote these two configurations by the orientation of spins in the center $\xi = \text{sgn}(S_z|_{r \rightarrow 0}) = \pm 1$. The example of the doublet of chiral BMPs with account for Dresselhaus spin-orbit interaction is shown in Fig. 8.

The presence of two spin textures with opposite orientation $\xi = \pm 1$ in the same layer modifies the expression for the charge contribution ρ_c to THE (14). Indeed, as $S_0 \approx 0$ the sign of the spin-chirality driven contributions $\Gamma_{1,2}$ to the carrier asymmetric scattering on the spin texture depends on its orientation and the contributions to ρ_c from textures with $\xi = \pm 1$ have opposite sign. We arrive at the modified expression for ρ_c accounting for both texture orientations $\xi = \pm 1$:

$$\rho_c = P_\xi \frac{1}{nec} (\phi_0 n_{sk}) \int (\Gamma_1 + \Gamma_2) \sin \theta d\theta, \quad (17)$$

$$P_\xi = \frac{n_+ - n_-}{n_+ + n_-},$$

where n_\pm are sheet densities of $\xi = \pm 1$ spin textures, respectively, $n_{sk} = n_+ + n_-$ is the total sheet density, P_ξ is the polarization of the texture array in terms of their orientations. Here we consider the dilute regime with $\tau_s = \tau_0$. It follows from (17), that observation of THE in chiral paramagnetic systems is possible only when there is an imbalance in the texture orientations i.e. $P_\xi \neq 0$.

Let us note, that for the positive texture polarization $P_\xi > 0$, the sign of ρ_c is different to that of ρ_c for magnetic skyrmions, or non-collinear rings in Fig. 1. Indeed, as we already mentioned, $\delta S_z < 0$ for the mag-

netic skyrmions case leading to $\rho_c > 0$. On the contrary, $\delta S_z > 0$ is positive for $\xi = +1$ shown in Fig. 8, so that $\rho_c < 0$.

V. SUMMARY

We have developed a theory of the topological Hall effect in a 2D system with randomly located chiral magnetic textures. We calculated THE resistivity ρ_{yx}^T on the basis of Boltzmann kinetic equation accounting for the carrier scattering asymmetry on a localized chiral spin texture. We have shown, that ρ_{yx}^T can be expressed as a sum of two contributions: $\rho_{yx}^T = \rho_c + \rho_a$. The first one ρ_c describes the transverse charge current due to spin-independent asymmetric scattering, while the second one ρ_a is spin-dependent and describes the spin Hall effect, contributing in its turn to the charge Hall current provided the free carriers are spin polarized. We have investigated the interplay between adiabatic and non-adiabatic regimes of free carriers scattering on spin textures. We predict the appearance of a local minimum in the dependence of ρ_{yx}^T on a skyrmion size associated with the crossover from charge Hall dominating to spin Hall dominating regime. The non-monotonic features were also found for the dependence of THE on the carriers Fermi energy. We have obtained general expressions for longitudinal and transverse components of the resistivity tensor upon the transition from dilute to dense skyrmion array in the particularly important case of the adiabatic scattering. Finally, we have clarified the role of spin-independent charge contribution to THE in dilute magnetic systems with zero background magnetization, showing that the sign of ρ_c is determined by the orientation of chiral spin texture in its center.

VI. ACKNOWLEDGMENTS

We thank V. Cross, A. Fert, D. Maccariello, N. Reyren for a very fruitful discussions and comments.

The work has been carried out under the financial support of Grants from the Russian Science Foundation (asymmetric scattering theory - project no. 17-12-01182; numerical calculations - project no. 17-12-01265) and from Russian Foundation of Basic Research (grant 18-02-00668). It was also supported by the Academy of Finland Grant No. 318500. K.S.D. and N.S.A. thank the Foundation for the Advancement of Theoretical Physics and Mathematics "BASIS".

Appendix A: Symmetry of scattering rates

In this Appendix we derive the relations (13) for the dimensionless asymmetric scattering rates $\mathcal{J}_{ss'}(\theta, \eta)$. The background polarization $\eta = \text{sgn}(S_0) = \pm 1$, it also determines the orientation of spins inside the core of

a chiral spin texture. The starting point is the time-reversal invariance, which states that if we make a replacement $\mathbf{S}(\mathbf{r}) \rightarrow -\mathbf{S}(\mathbf{r})$, then the scattering rate from $(\mathbf{p}', s') \rightarrow (\mathbf{p}, s)$ with a scattering angle $\theta = \varphi - \varphi'$ is equal to that of $(-\mathbf{p}, \bar{s}) \rightarrow (-\mathbf{p}', \bar{s}')$ with the scattering angle $-\theta$ (\bar{s} denotes the carrier spin state opposite to s). The replacement $\mathbf{S}(\mathbf{r}) \rightarrow -\mathbf{S}(\mathbf{r})$ leads to $\eta \rightarrow -\eta$, $\varkappa \rightarrow \varkappa$, and $\gamma \rightarrow \gamma + \pi$. Collecting these operations together we obtain:

$$\mathcal{G}_{ss'}(\theta, \eta) + \mathcal{J}_{ss'}(\theta, \eta) = \mathcal{G}_{\bar{s}'\bar{s}}(-\theta, -\eta) + \mathcal{J}_{\bar{s}'\bar{s}}(-\theta, -\eta) \quad (\text{A1})$$

Taking into account that $\mathcal{G}_{ss'}(\theta, \eta) = \mathcal{G}_{ss'}(-\theta, \eta)$ and $\mathcal{J}_{ss'}(\theta, \eta) = -\mathcal{J}_{ss'}(-\theta, \eta)$ we get that symmetric $\mathcal{G}_{ss'}$ and asymmetric $\mathcal{J}_{ss'}$ rates should satisfy:

$$\begin{aligned} \mathcal{G}_{ss'}(\theta, \eta) &= \mathcal{G}_{\bar{s}'\bar{s}}(\theta, -\eta), \\ \mathcal{J}_{ss'}(\theta, \eta) &= -\mathcal{J}_{\bar{s}'\bar{s}}(\theta, -\eta). \end{aligned} \quad (\text{A2})$$

We further focus on $\mathcal{J}_{ss'}$. The relations (A2) couple the two scattering channels with the opposite spin orientations. For the spin-conserving channels we have:

$$\mathcal{J}_{\uparrow\uparrow}(\theta, \eta) = -\mathcal{J}_{\downarrow\downarrow}(\theta, -\eta). \quad (\text{A3})$$

Let us introduce the symmetrized and antisymmetrized combinations of $\mathcal{J}_{\uparrow\uparrow}(\theta, \eta)$, $\mathcal{J}_{\uparrow\uparrow}(\theta, -\eta)$ with respect to η :

$$\begin{aligned} \Gamma(\theta, \eta) &= \frac{1}{2} (\mathcal{J}_{\uparrow\uparrow}(\theta, \eta) - \mathcal{J}_{\uparrow\uparrow}(\theta, -\eta)), \\ \Pi(\theta) &= \frac{1}{2} (\mathcal{J}_{\uparrow\uparrow}(\theta, \eta) + \mathcal{J}_{\uparrow\uparrow}(\theta, -\eta)). \end{aligned} \quad (\text{A4})$$

Since the background polarization $\eta = \pm 1$ can take only two values, it is obvious that the function Π does not depend on η , while $\Gamma(-\eta) = -\Gamma(\eta)$. Let us extract the dependence of Γ on η in the explicit form: $\Gamma(\eta, \theta) \equiv \eta\Gamma_1(\theta)$, where Γ_1 depends only on θ and on the energy of an incident electron. Expressing the rates of the spin-conserving channels and using the symmetry (A3) we arrive at the relations (13):

$$\begin{aligned} \mathcal{J}_{\uparrow\uparrow}(\theta, \eta) &= \eta\Gamma_1(\theta) + \Pi(\theta), \\ \mathcal{J}_{\downarrow\downarrow}(\theta, \eta) &= \eta\Gamma_1(\theta) - \Pi(\theta). \end{aligned} \quad (\text{A5})$$

As for the spin-flip channels, there is an additional symmetry $\mathcal{J}_{\uparrow\downarrow}(\theta, \eta) = \mathcal{J}_{\downarrow\uparrow}(\theta, \eta)$ as the Hamiltonian is hermitian, this symmetry leads to the absence of a spin Hall part:

$$\mathcal{J}_{\downarrow\uparrow}(\theta, \eta) = \mathcal{J}_{\uparrow\downarrow}(\theta, \eta) = \eta\Gamma_2(\theta), \quad (\text{A6})$$

where $\Gamma_2(\theta)$ does not depend on η .

* Electronic address: denisokonstantin@gmail.com

- ¹ N. Nagaosa and Y. Tokura, *Nature Nanotechnology* **8**, 899 (2013).
- ² A. Fert, V. Cros, and J. Sampaio, *Nature nanotechnology* **8**, 152 (2013).
- ³ A. Fert, N. Reyren, and V. Cros, *Nature Reviews Materials* **2**, 17031 (2017).
- ⁴ R. Wiesendanger, *Nature Reviews Materials* **1**, 16044 (2016).
- ⁵ K. Ahadi, L. Galletti, and S. Stemmer, *Applied Physics Letters* **111**, 172403 (2017).
- ⁶ M. Leroux, M. J. Stolt, S. Jin, D. V. Pete, C. Reichhardt, and B. Maiorov, arXiv:1805.05267 (2018).
- ⁷ A. Soumyanarayanan, M. Raju, A. G. Oyarce, A. K. Tan, M.-Y. Im, A. P. Petrović, P. Ho, K. Khoo, M. Tran, C. Gan, et al., *Nature materials* **16**, 898 (2017).
- ⁸ M. Raju, A. Yagil, A. Soumyanarayanan, A. K. Tan, A. Almoalem, O. Auslaender, and C. Panagopoulos, arXiv preprint arXiv:1708.04084 (2017).
- ⁹ C. S. Spencer, J. Gayles, N. A. Porter, S. Sugimoto, Z. Aslam, C. J. Kinane, T. R. Charlton, F. Freimuth, S. Chadov, S. Langridge, et al., *Phys. Rev. B* **97**, 214406 (2018).
- ¹⁰ A. Neubauer, C. Pfleiderer, B. Binz, A. Rosch, R. Ritz, P. G. Niklowitz, and P. Böni, *Phys. Rev. Lett.* **102**, 186602 (2009).
- ¹¹ Y. Li, N. Kanazawa, X. Z. Yu, A. Tsukazaki, M. Kawasaki,

- M. Ichikawa, X. F. Jin, F. Kagawa, and Y. Tokura, *Phys. Rev. Lett.* **110**, 117202 (2013).
- ¹² B. J. Chapman, M. G. Grossnickle, T. Wolf, and M. Lee, *Phys. Rev. B* **88**, 214406 (2013).
- ¹³ C. Sürgers, G. Fischer, P. Winkel, and H. v. Löhneysen, *Nature communications* **5** (2014).
- ¹⁴ B. Ueland, C. Miclea, Y. Kato, O. Ayala-Valenzuela, R. McDonald, R. Okazaki, P. Tobash, M. Torrez, F. Ronning, R. Movshovich, et al., *Nature communications* **3**, 1067 (2012).
- ¹⁵ F. W. Fabris, P. Pureur, J. Schaf, V. N. Vieira, and I. A. Campbell, *Phys. Rev. B* **74**, 214201 (2006).
- ¹⁶ T. Taniguchi, K. Yamanaka, H. Sumioka, T. Yamazaki, Y. Tabata, and S. Kawarazaki, *Phys. Rev. Lett.* **93**, 246605 (2004).
- ¹⁷ Y. Ohuchi, Y. Kozuka, M. Uchida, K. Ueno, A. Tsukazaki, and M. Kawasaki, *Phys. Rev. B* **91**, 245115 (2015).
- ¹⁸ D. Maccariello, W. Legrand, N. Reyren, K. Garcia, K. Bouzehouane, S. Collin, V. Cros, and A. Fert, *Nature Nanotechnology* pp. 1748–3395 (2018).
- ¹⁹ L. N. Oveshnikov, V. A. Kulbachinskii, A. B. Davydov, B. A. Aronzon, I. V. Rozhansky, N. S. Averkiev, K. I. Kugel, and V. Tripathi, *Scientific Reports* **5**, 17158 (2015).
- ²⁰ C. Liu, Y. Zang, W. Ruan, Y. Gong, K. He, X. Ma, Q.-K. Xue, and Y. Wang, *Phys. Rev. Lett.* **119**, 176809 (2017).
- ²¹ N. Kanazawa, M. Kubota, A. Tsukazaki, Y. Kozuka, K. S. Takahashi, M. Kawasaki, M. Ichikawa, F. Kagawa, and

- Y. Tokura, Phys. Rev. B **91**, 041122 (2015).
- ²² S. Mühlbauer, B. Binz, F. Jonietz, C. Pfleiderer, A. Rosch, A. Neubauer, R. Georgii, and P. Bni, Science **323**, 915 (2009).
- ²³ W. Münzer, A. Neubauer, T. Adams, S. Mühlbauer, C. Franz, F. Jonietz, R. Georgii, P. Böni, B. Pedersen, M. Schmidt, et al., Phys. Rev. B **81**, 041203 (2010).
- ²⁴ P. Bruno, V. K. Dugaev, and M. Taillefumier, Phys. Rev. Lett. **93**, 096806 (2004).
- ²⁵ B. Binz and A. Vishwanath, Physica B: Condensed Matter **403**, 1336 (2008).
- ²⁶ J. Ye, Y. B. Kim, A. J. Millis, B. I. Shraiman, P. Majumdar, and Z. Tešanović, Phys. Rev. Lett. **83**, 3737 (1999).
- ²⁷ Y. Lyanda-Geller, S. H. Chun, M. B. Salamon, P. M. Goldbart, P. D. Han, Y. Tomioka, A. Asamitsu, and Y. Tokura, Phys. Rev. B **63**, 184426 (2001).
- ²⁸ P. B. Ndiaye, C. A. Akosa, and A. Manchon, Phys. Rev. B **95**, 064426 (2017).
- ²⁹ G. Tatara, H. Kohno, J. Shibata, Y. Lemaho, and K.-J. Lee, Journal of the Physical Society of Japan **76**, 054707 (2007).
- ³⁰ S. S.-L. Zhang and O. Heinonen, Phys. Rev. B **97**, 134401 (2018).
- ³¹ Y. Taguchi, Y. Oohara, H. Yoshizawa, N. Nagaosa, and Y. Tokura, Science **291**, 2573 (2001).
- ³² K. Nakazawa, M. Bibes, and H. Kohno, Journal of the Physical Society of Japan **87**, 033705 (2018).
- ³³ H. Ishizuka and N. Nagaosa, Science Advances **4**, eaap9962 (2018).
- ³⁴ K. Denisov and N. Averkiev, Applied Physics Letters **112**, 162409 (2018).
- ³⁵ K. S. Denisov, I. V. Rozhansky, N. S. Averkiev, and E. Lähderanta, Scientific Reports **7**, 17204 (2017).
- ³⁶ K. S. Denisov, I. V. Rozhansky, N. S. Averkiev, and E. Lähderanta, Phys. Rev. Lett. **117**, 027202 (2016).
- ³⁷ G. Tatara and H. Kawamura, J. Phys. Soc. of Japan **71**, 2613 (2002).
- ³⁸ K. Nakazawa and H. Kohno, J. Phys. Soc. of Japan **83**, 073707 (2014).
- ³⁹ M. Onoda, G. Tatara, and N. Nagaosa, Journal of the Physical Society of Japan **73**, 2624 (2004).
- ⁴⁰ I. S. Lobanov, H. Jónsson, and V. M. Uzdin, Physical Review B **94**, 174418 (2016).
- ⁴¹ C. Moreau-Luchaire, C. Moutafis, N. Reyren, J. Sampaio, C. Vaz, N. Van Horne, K. Bouzehouane, K. Garcia, C. Deranlot, P. Warnicke, et al., Nature nanotechnology **11**, 444 (2016).
- ⁴² A. Soumyanarayanan, N. Reyren, A. Fert, and C. Panagopoulos, Nature **539**, 509 (2016).
- ⁴³ A. Bogdanov and A. Hubert, Journal of magnetism and magnetic materials **138**, 255 (1994).
- ⁴⁴ A. Bogdanov and A. Hubert, Journal of magnetism and magnetic materials **195**, 182 (1999).
- ⁴⁵ A. Belavin and A. Polyakov, JETP lett **22**, 245 (1975).
- ⁴⁶ L. Brey, Nano letters **17**, 7358 (2017).
- ⁴⁷ P. F. Bessarab, G. P. Müller, I. S. Lobanov, F. N. Rybakov, N. S. Kiselev, H. Jónsson, V. M. Uzdin, S. Blügel, L. Bergqvist, and A. Delin, Scientific reports **8**, 3433 (2018).
- ⁴⁸ K. S. Denisov and N. S. Averkiev, JETP Letters **99**, 400 (2014).
- ⁴⁹ Y. Berkovskaya, B. Gel'mont, and E. Tsidil'kovskii, Sov. Phys.-Semiconductors **22**, 539 (1998).
- ⁵⁰ Y. Berkovskaya, E. Vakhobova, B. Gel'mont, and I. Merkulov, JETP **67**, 750 (1988).
- ⁵¹ K. Denisov, I. Rozhansky, M. Potkina, I. Lobanov, E. Lähderanta, and V. Uzdin, arXiv preprint arXiv:1803.06124 (2018).
- ⁵² C. P. Moca, B. L. Sheu, N. Samarth, P. Schiffer, B. Janko, and G. Zarand, Phys. Rev. Lett. **102**, 137203 (2009).
- ⁵³ M. Kamal and G. Murthy, Physical review letters **71**, 1911 (1993).